Self-assembly of micro-machining systems powered by Janus micro-motors

Claudio Maggi[1],[a] Filippo Saglimbeni[1], Juliane Simmchen,
Jaideep Katuri, Samuel Sánchez[2], and Roberto Di Leonardo[1,3]
[1] *Dipartimento di Fisica, Università di Roma "Sapienza", I-00185, Roma, Italy*
[2] *Some affiliation and*
[3] *NANOTEC-CNR, Institute of Nanotechnology,*
Soft and Living Matter Laboratory, Piazzale A. Moro 2, I-00185, Roma, Italy
(Dated: July 22, 2015)

Integration of active matter in larger micro-devices can provide an embedded source of propulsion and lead to self-actuated micromachinig systems that do not rely on any external power or control apparatus. Here we demonstrate that Janus colloids can self-assemble around a micro-fabricated rotor in reproducible configurations with a high degree of spatial and orientational order. The final configuration maximizes the torque applied on the rotor leading to a unidirectional and steady rotating motion. We discuss how the interplay between geometry and dynamical behaviour consistently leads to the self-assembly of autonomous micromotors starting from randomly distributed building blocks.

Several developments for defined manipulation, transport and assembly of micro-objects have been presented. One of the earliest approaches were microelectromechanical systems(MEMS) based microgripper [1]. They represent a very versatile strategy that might be used for handling fragile objects, but it also allows the displacement of miniature devices in the order of millimeter [2, 3]. Non-contact manipulation is achieved by electrostatic actuators evolved from tip like actuators [4] to cilia inspired structures [5] taking benefit of electrostatic interaction and low Reynolds numbers. To manipulate magnetic microobjects the use of magnetic fields presents an elegant solution[6–8]. Not limited to magnetic material is the use optical tweezers that allow very precise displacement of dielectric microobjects [9]. Those methods accurately control grasping forces in order to avoid any damage to the small-size delicate objects, yet require in general very large and complex devices and conditions that are usually met only in research laboratories. Previously several groups presented approaches to move cargo employing micromotors benefitting from phenomena as cooperation or collective transport, as for example Tottori et al. presented helical micromachines with microholders that used mechanical contact to transport passive particles [8]. Catalytic rod- and tube-shaped micromotors were shown to be useful for cargo transport [8, 12–15], as well as Janus particles that have been shown to move particles larger than their size [16, 17]. Living kinds of active matter such as bacteria [18, 19, 24, 25] and sperm cells [20] was shown to be captured by different microstructures. Bacterial power has been studied theoretically and their usage predicted [21, 22] and experimentally proven for different kind of bacteria such as Serratia marcescens [25], *E. Coli* [21, 23] and *Bacillus subtilis* [22]. Suspensions of bacteria or synthetic microswimmers show fascinating collective behaviors which depending on concentration of bacteria might give rise to hydrodynamic turbulence (swirling state). Kaiser et al. found that both polar ordering and swirl shielding inside a wedge structure can yield an optimal transport velocity which becomes even bidirectional at high concentrations [22]. All above phenomena take place only at relatively large bacterial concentrations [26] and always involve a partial rectification that is inevitably accompanied by a high degree of randomness and low reproducibility.

Here we demonstrate that a small and well defined number of artificial micromotors can self-organize in highly ordered configurations around a larger passive micro-object and propel it in a steady unidirectional motion. The highly deterministic character of the proposed self-assembly strategy is based on a previously reported dynamical behavior of Janus particles colliding with solid obstacles. When approaching a step structure, the phoretic interaction of the self-generated solute gradient with both, the substrate and the step/wall [cite our paper], particles orient their symmetry axis parallel to the side wall. By choosing a convenient relationship between the lengths of the sides of a microgear, we force the active particles to dock on the gears in a well defined position and orientation. In this manuscript we study the effect of number and orientation of the particles on the motion of the microgears. We envision that the use of Janus particles to empower the motion of microobject such as gears could pave the way for more applicable micromachines.

The active component is made of platinum-coated silica Janus particles (diameter $a = 5$ μm) that can self-propel in a mixture deionized water and hydrogen peroxide. The passive component is a micro fabricated gear having six asymmetric teeth with an external radius of 8 μm. The two components, initially in a deionized water

[a]claudio.maggi@roma1.infn.it

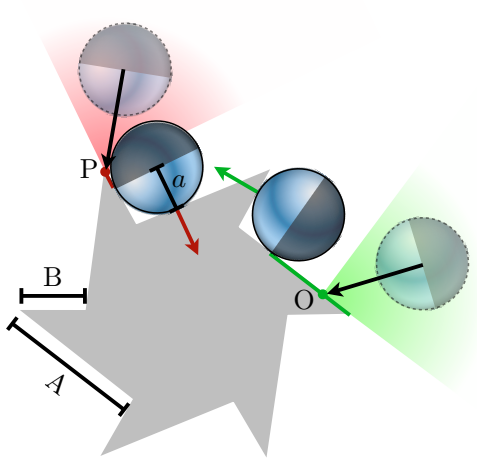

FIG. 1. Schematic representation of the two possible docking events leading to a Janus particle applying a constant propulsion to the micro-gear.

solution, are mixed on a plasma-cleaned glass coverslip where they sediment displaying rotational and translational Brownian motion restricted to the proximity of the surface. The typical final area concentrations are XXX μm^{-2} for Janus particles and XXX for micro-gears. When hydrogen-peroxide (H_2O_2, 5% concentration) is added to the sample we immediately observe active motion of the Janus particles. The sample is observed by bright-field microscopy recording digital images at a frame rate of 50 fps (see Experimental Section). Acquisition of digital frames and analysis are always performed few seconds after the addition of fresh H_2O_2 to the sample in order to maintain the activity of the Janus particles approximately constant for all measurements. After few seconds following H_2O_2 addition, one or more Janus particles collide with each microgear. The active particles align their propelling direction along the side of the gear and, depending on their incident angle with the edge normal, either leave the structure or slide along the edge until they get stuck on a corner. Two distinct final configurations are possible. A particles collides in O coming from the green shaded region, aligns and then eventually docks propelling the structure in Fig in an anticlockwise direction. The probability of events of this type is proportional to the length A-a of the green segment representing the locus of possible impact points O. A second docked state occurs when a particles collides in P coming from the red region and gets stuck pushing the structure in the opposite direction and with a lower torque. Analogously the probability of these events is proportional to B-a. Therefore the majority of fully occupied structures will have all particles pushing in the same anticlockwise direction, while the fraction of "wrong" assemblies where for example one particle points in the opposite direction is only B-a/A-a with the optimal situation being B a. In our case B=XX, A=XX so that only 1 structure among 10 is expected to form with a misoriented particle. The alignment observed here is consistent with previous experiments on the alignment of Janus particles along extended linear obstacles of various thickness and it has been ascribed to the influence of the boundary onto the phoretic slip-flow generated by the particle [REF!].

Fig. 2 reports a typical docking event which is composed of three main stages: in Fig. 2(a) the particle moves freely pointing towards a gear, Fig. 2(b) the particle touches the long edge and aligns along it, finally in Fig. 2(c) the particle slides along the long edge until it arrives at the short edge and starts pushing with maximal applied torque. To quantify these effects we perform tracking of the gear and the Janus particle by using a shape-recognition algorithm. We define particle and gear edge orientation as indicated by arrows in Figure. The angle formed by these two vectors with a common horizontal reference is shown as dashed lines in Fig. 2(d). Before collision the Janus particle only shows moderate Brownian(?) fluctuations of its orientation (approach stage) while the gear rotates at approximately constant speed under the action of two well-aligned particles. After collision we observe reorientation of the particle (alignment stage). Once the alignment is complete and the particle reaches the short blocking edge the two orientation angles merge on the same curve and the assembly moves as a rigid body (push stage).

In the latter regime we observe a clear increase of the rotational speed of the gear, with respect to the approach stage, as shown by linear fits (dashed lines) in Fig. 2(d).

Once the particle is trapped in the corner of the gear its orientation is stably locked around the orientation of the long edge of the gear showing only small fluctuations. This has been quantified by tracking for at least 5 s the orientation of about 30 different Janus particle fitting in the corners of about 10 different microgears and the orientation corresponding nearest long edge. In Fig. 2(e) we plot the histogram of the angular difference between the the orientation angle of the Janus particle and the orientation angle of its nearest long edge (see arrows in the inset of Fig. 2(d)). The probability distribution of this angular difference is well fitted by a Gaussian (full line in Fig. 2(e)) resulting in an average angular fluctuations of 5.7 ± 0.8 degrees. The amplitude of fluctuations is very similar for all Janus particles tracked, a sample of these fluctuations is shown in Fig. 2(f) where we report the angular difference for one single particle for a time span of 6 s.

As mentioned above when a Janus particle collides, aligns and locks to the gear we usually see a clear increase of the rotational speed. Occasionally we also observe that a stuck Janus particle reorients for a Brownian fluctuation and leaves the structure. These events are instead accompanied by a decrease in rotational speed of the gear. In both cases the change of the rotational

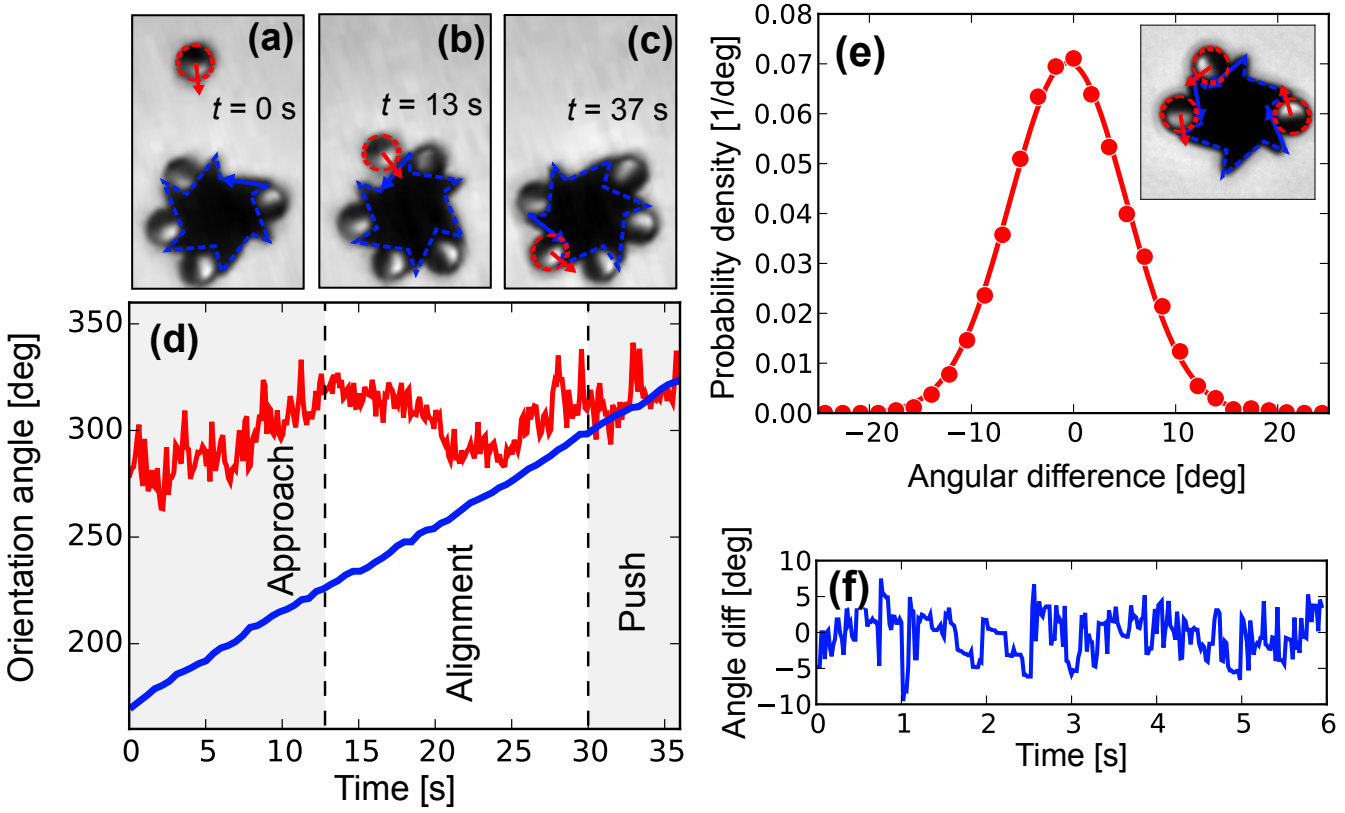

FIG. 2. **(a)** One Janus particle approaches the gear, the dashed lines are results of tracking and the arrows indicate the orientation vector of the gear and the Janus particle. **(b)** The Janus particle enters in contact with one of the long-teeth of the gear and aligns along it. **(c)** The Janus particle fits and remains in the corner formed by the short and the long tooth of the gear. **(d)** Temporal evolution of the orientation angle of the gear (red line) and of the Janus particle (gray line), during the approach, alignment and pushing stages. Dashed lines are linear fits of the gear's angle in the approach and push stages. **(e)** Probability distribution of the angle formed by the orientation vector of the Janus particle and the orientation vector of nearest long-tooth edge of the gear (see inset). **(f)** Typical fluctuations of the angle formed by the orientation vector of the Janus particle and the corresponding long-tooth edge as a function of time.

speed is approximately proportional to free propulsion speed of the Janus particle far from the structure. We measure the change of rotational speed and the speed of the incoming/leaving Janus for six different attaching/detaching events happening at low Janus particles density (when at most three Janus particles are in contact with the gear). These measurements are obtained by tracking gears and particles for at least 3 s. The results are shown in Fig. 3 where we plot the change of rotation speed of the microgear, after one single event, as a function of the speed of the particle. The angular coefficient of the linear fit shown in Fig. 3 (full line) results to be $\alpha = 1.1 \pm 0.1$ deg/μm. A rough estimate of this factor can be obtained if we assume that a pushing Janus particle exerts a force of order $f = 6\pi\eta a v$ where v is the particle's speed and η the viscosity of the solvent. This force will generate a torque $T = fr$, with r the radius of the microgear. By approximating the rotational viscous drag of the Janus-gear structure as $\Gamma \approx 8\pi\eta r^3$ we obtain the contribution $\Delta\Omega$ of one single particle to the gear rotational speed as $\Delta\Omega = T/\Gamma = \alpha\, v$, where $\alpha = (3/4)a/r^2 \approx 2.5$ deg/μm which is of the same order of magnitude of the measured value.

Upon increasing the Janus particles density the probability of finding more teeth occupied on each single gear grows significantly. By increasing the overall number of Janus particles per unit surface of a about a factor ten (from 0.022 ± 0.06 to 0.19 ± 0.02 area fraction) we observe that the number of particles fitting in the microgear's teeth increases gradually from 1 to 6 (maximum occupancy). This is shown in Fig. 4(a),(b) and (c) where we show typical configuration at low, intermediate and high particles densities respectively. Upon increasing the number of Janus particles in contact with the gear from 1 to 2 to 3 we observe a reproducible increase of the angular speed of the gear as seen by comparing the angle spanned by the gear with 2 and 3 particles in 14 s (shown in Fig. 4(a) and (b) respectively). We also observe that the center of the gear shows always a displacement limited to few microns in the measurement time (small ar-

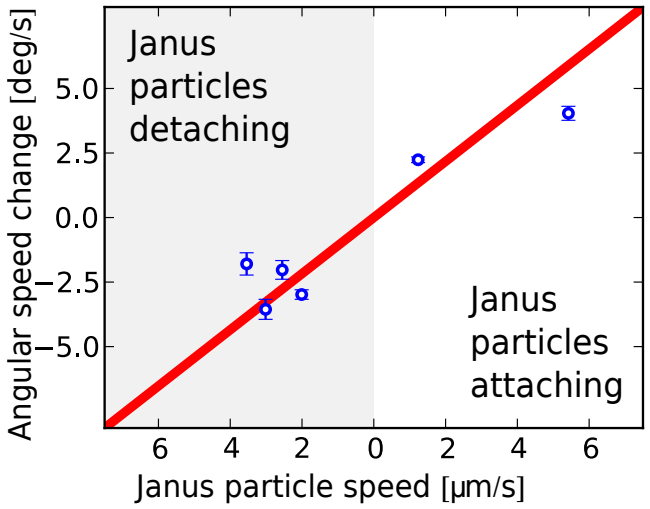

FIG. 3. **(a)** Change in angular speed (circles) of the micro-gear when one single Janus particle attaches (right) or detaches (left) as a function of the speed of the Janus particle measure before/after the attachment/detachment respectively. The full line is a linear fit passing through zero.

rows in Fig. 4(a),(b) and (c)). Upon further increasing the particle density, for a number of occupied sites going from 4 to 6 Janus particles, we observe instead a decrease of rotation rates. This non monotonic behaviour of rotational speeds with the number N of occupied sites is already visible in Fig. 4 for $N = 2, 3, 6$ and summarised in Fig. 5 for all values of N.

These last are obtained by tracking the orientation angles of about 10 different microgears for at least 5 s. By averaging the measurement of rotational speed obtained for the same number of particles in contact (thick line in Fig. 5) we obtain a clear trend confirming the non-monotonic behaviour of gear rotational speed described above (see Fig. 4). If the number of Janus particle in contact with the gear is limited to 3 the rotational speed increase systematically with the number of particles in contact. The magnitude of this increase is also consistent with the estimate of the contribution given by each particle to the rotational speed shown in Fig 3. By using the measured value of $\alpha = 1.1 \pm 0.1$ deg/μm and the measured average speed of all Janus particles tracked $v = 2.6 \pm 0.4$ μm/s, we expect the angular speed of the gear Ω to grow linearly with the number n of particles in contact as $\Omega = \beta\, n$ where $\beta = \alpha\, v = 2.8 \pm 0.5$ deg/s which is shown as a shaded area in Fig. 5, which captures the trend of the data up to $n = 3$. Differently for $n \geq 4$ the Ω stops increasing and then decreases. At a fixed fuel concentration we would expect that the rotational speed could never exceed the value v/r for which the free propulsion speed of the particle equals the linear speed of the rotor's edge. Additionally the total drag of the rotating body increases with N so that a slow saturation to the maximum speed would be expected. The observed speed decrease at larger N values should most probably be attributed to a progressive reduction of fuel concentration due to both the local and global increase in the number density of Janus particles depleting hydrogen peroxide.

We demonstrated the self-organization of self-propelled Janus particles to power passive larger engineered objects, i.e. micro-gears. We characterized the entrance and docking of the Janus particle on the gear, as well as the orientation during the motion, observing a correlation on the angular velocity of the gear with the number of particles attached. An increase of velocity is registered with increasing particle number from 1 to 3 particles, resulting in a plateau from 3-4 particles and decreasing after addition of more particles. We theoretically derived possible origin of this behavior. This approach presents an elegant way to achieve the displacement of passive micro-objects. We expect the smart interaction of active particles with confining walls, like those engineered on the micro-gears, providing a propulsion force to micro-objects will be applied to engineering of micromachines in the near future.

EXPERIMENTAL SECTION

Janus particles synthesis. Sample preparation. Janus particles were obtained by drop casting of a suspension of spherical silica colloids (5 μm diameter, Sigma Aldrich) on an oxygen-plasma cleaned glass slide followed by slow evaporation of the solvent and placed in an ebeam system. High vacuum was applied and subsequently a monolayer of 2 nm Ti was evaporated to guarantee good adhesion of the 7 nm Pt for catalytic properties. To release particles from the glass slides into DI water, short ultrasound pulses were sufficient.

Substrate treatment. To obtain clean and hydrophilic substrates glass slides were cleaned with alcohol, dried and treated during 5 min in a Diener oxygen plasma machine, substrates were used immediately after this procedure. .

Gears microfabrication. The fabrication starts with the spin-coating and baking (200°C) of LOR3B/SU-8 (200 nm/4 μm on a silicon wafer). An amorphous carbon film (100 nm) is then deposited on the SU-8 by sputtering. Subsequently, LOR3B/S1813 (200 nm/1.5 μm) are spin-coated on the carbon layer, and laser lithography is performed to obtain the negative pattern of the microgears in the LOR3B/S1813 bilayer. After the evaporation of 100 nm chrome, the LOR3B/S1813 bilayer is removed by N-methyl-2-pyrrolidone, leaving chrome microgears on the carbon layer. The SU-8/carbon layer is then etched by Reactive Ion Etching (RIE) in oxygen plasma; the chrome microgears act as etching mask and transfer their shape onto the SU-8;

the etching process is anisotropic and produces SU-8 vertical walls. A finalized SU-8 microgear is depicted in Fig. 2a after chrome removal in chrome-etch solution. The microgears are finally released from the wafer by PG-remover, which dissolves the sacrificial LOR3B layer at the bottom of the microgears (see Supplemental Material for a detailed scheme of microfabbrication).

Optical setup Bright-field microscopy is performed by using an inverted optical microscope (Nikon TE-2000U) equipped with a 20× (NA=0.5) objective. Images are recorded with a high-sensitivity CMOS camera (Hamamatsu Orca Flash 2.8). In each measurement we record videos at least 3 s long (∼ 150 frames) up to a maximum of about 30 s (∼1500 frames).

[1] Chang-Jin Kim; Pisano, A. P. M., R.S.; Lim, M.G: Polysilicon microgripper,. In Solid-State Sensor and Actuator Workshop, 1990; pp 48-51.

[2] Nah, S. K.; Zhong, Z. W.: A microgripper using piezoelectric actuation for micro-object manipulation. Sensors and Actuators A: Physical 2007, 133, 218-224.

[3] Yukun Jia, Q. X.: MEMS Microgripper Actuators and Sensors: The State-of-the-Art Survey Recent Patents on Mechanical Engineering 2013, 6.

[4] Haliyo, D. S. a. R., Y. and Regnier, S.: Manipulation of micro-objects using adhesion forces and dynamical effects In Robotics and Automation, 2002. Proceedings. ICRA '02. IEEE International Conference on 2002; Vol. 2.

[5] Chieh, C.; Chia-Fang, C.; Cheng-Hsiang, L.; Cheng-Hsien, L.: A lobster-sniffing-inspired method for micro-objects manipulation using electrostatic micro-actuators. J. Micromech. Microeng. 2005, 15, 812.

[6] Peyer, K. E.; Zhang, L.; Nelson, B. J.: Bio-inspired magnetic swimming microrobots for biomedical applications. Nanoscale 2013, 5, 1259-1272.

[7] Huang, T.-Y.; Qiu, F.; Tung, H.-W.; Peyer, K. E.; Shamsudhin, N.; Pokki, J.; Zhang, L.; Chen, X.-B.; Nelson, B. J.; Sakar, M. S.: Cooperative manipulation and transport of microobjects using multiple helical microcarriers. RSC Advances 2014, 4, 26771-26776.

[8] Tottori, S.; Zhang, L.; Qiu, F. M.; Krawczyk, K. K.; Franco-Obregon, A.; Nelson, B. J.: Magnetic Helical Micromachines: Fabrication, Controlled Swimming, and Cargo Transport. Adv. Mater. (Weinheim, Ger.) 2012, 24, 811-816.

[9] Maruo, S.: Manipulation of Microobjects by Optical Tweezers. In Microfluidic Technologies for Miniaturized Analysis Systems; Hardt, S., Schönfeld, F., Eds.; Springer US, 2007; pp 275-314.

[10] Mondal, A.; Roy, B.; Banerjee, A.: Generation of microswimmers from passive Brownian particles in a spherically aberrated optical trap. Opt. Express 2015, 23, 8021-8028.

[11] Volpe, G.; Kurz, L.; Callegari, A.; Volpe, G.; Gigan, S.: Speckle optical tweezers: micromanipulation with random light fields. Opt. Express 2014, 22, 18159-18167.

[12] Burdick, J.; Laocharoensuk, R.; Wheat, P. M.; Posner, J. D.; Wang, J.: Synthetic nanomotors in microchannel networks: Directional microchip motion and controlled manipulation of cargo. J. Am. Chem. Soc. 2008, 130, 8164-8165.

[13] Sundararajan, S.; Lammert, P. E.; Zudans, A. W.; Crespi, V. H.; Sen, A.: Catalytic motors for transport of colloidal cargo. Nano Lett. 2008, 8, 1271-1276.

[14] Solovev, A. A.; Sanchez, S.; Pumera, M.; Mei, Y. F.; Schmidt, O. G.: Magnetic Control of Tubular Catalytic Microbots for the Transport, Assembly, and Delivery of Micro-objects. Adv. Funct. Mater. 2010, 20, 2430-2435.

[15] Sanchez, S.; Solovev, A. A.; Harazim, S. M.; Schmidt, O. G.: Microbots Swimming in the Flowing Streams of Microfluidic Channels. J. Am. Chem. Soc. 2011, 133, 701-703.

[16] Simmchen, J.; Baeza, A.; Ruiz, D.; Esplandiu, M. J.; Vallet-RegÃ, M.: Asymmetric Hybrid Silica Nanomotors for Capture and Cargo Transport: Towards a Novel Motion-Based DNA Sensor. Small 2012, 8, 2053-2059.

[17] Baraban, L.; Makarov, D.; Streubel, R.; Monch, I.; Grimm, D.; Sanchez, S.; Schmidt, O. G.: Catalytic Janus Motors on Microfluidic Chip: Deterministic Motion for Targeted Cargo Delivery. ACS Nano 2012, 6, 3383-3389.

[18] Kaiser, A.; Popowa, K.; Wensink, H. H.; Löwen, H.: Capturing self-propelled particles in a moving microwedge. Physical Review E 2013, 88, 022311.

[19] Kaiser, A.; Wensink, H. H.; Löwen, H.: How to Capture Active Particles. Phys. Rev. Lett. 2012, 108, 268307.

[20] Guidobaldi, A.; Jeyaram, Y.; Berdakin, I.; Moshchalkov, V. V.; Condat, C. A.; Marconi, V. I.; Giojalas, L.; Silhanek, A. V.: Geometrical guidance and trapping transition of human sperm cells. Physical Review E 2014, 89, 032720.

[21] Angelani, L.; Maggi, C.; Bernardini, M. L.; Rizzo, A.; Di Leonardo, R.: Effective Interactions between Colloidal Particles Suspended in a Bath of Swimming Cells. Physical Review Letters 2011, 107, 138302.

[22] Kaiser, A.; Peshkov, A.; Sokolov, A.; ten Hagen, B.; Löwen, H.; Aranson, I. S.: Transport Powered by Bacterial Turbulence. Physical Review Letters 2014, 112, 158101.

[23] Di Leonardo, R.; Angelani, L.; Dell'Arciprete, D.; Ruocco, G.; Iebba, V.; Schippa, S.; Conte, M. P.; Mecarini, F.; De Angelis, F.; Di Fabrizio, E.: Bacterial ratchet motors. Proc. Natl. Acad. Sci. U. S. A. 2010, 107, 9541-9545.

[24] Douglas B. Weibel, P. G., Declan Ryan, Willow R. DiLuzio, Michael Mayer, Jennifer E. Seto, and George M. Whitesides: Microoxen: Microorganisms to move microscale loads. PNAS 2005, 102, 11963-11967.

[25] Steager, E.; Kim, C.-B.; Patel, J.; Bith, S.; Naik, C.; Reber, L.; Kim, M. J.: Control of microfabricated structures powered by flagellated bacteria using phototaxis. Applied Physics Letters 2007, 90, 263901.

[26] Sokolov, A.; Apodaca, M. M.; Grzybowski, B. A.; Aranson, I. S.: Swimming bacteria power microscopic gears. Proceedings of the National Academy of Sciences 2010, 107, 969-974.

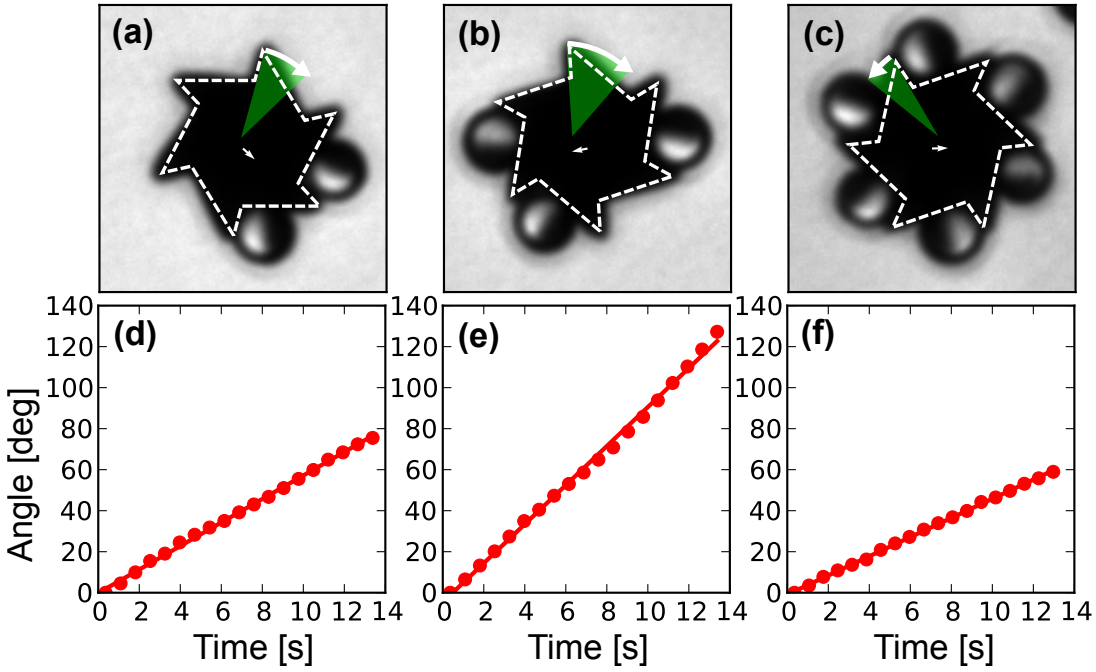

FIG. 4. **(a)** One microgear pushed by two Janus particles. The dashed line represents the results of the tracking. The green shaded area represents the angle spanned in a time of 4 s. The small white arrow represents the displacement of the center of mass in a time span of 14 s. **(b)** One microgear pushed by three Janus particles. **(c)** One microgear pushed by six Janus particles, note that this gears rotates counterclockwise having opposite orientation. Note that in (a),(b) and (c) the Janus particles have always their propulsion directions aligned with the long teeth of the microgear. **(d)**, **(e)**, and **(f)** Evolution of the angle (circles) of the gear with time for the gears shown in (a),(b) and (c) respectively. The lines represents linear fits of the data.

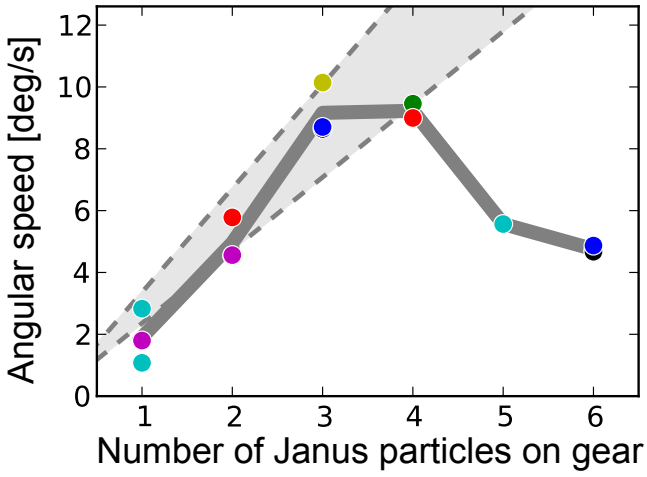

FIG. 5. Rotation speed of different gears as a function of the number of Janus particles in contact with the gear (regardless of their specific location), each circle represents a different gear. The full line represents an average over all the gears having the same number of Janus particles in contact. The shaded area is the predicted angular speed from single-event observation (Fig. 3, see text).